THE ASTROPHYSICAL JOURNAL, 550:724–736, 2001 April 1

ULTRAVIOLET LINE SPECTRA OF METAL-POOR STAR-FORMING GALAXIES

CLAUS LEITHERER
Space Telescope Science Institute,[1] 3700 San Martin Drive, Baltimore, MD 21218; leitherer@stsci.edu
JOÃO R. S. LEÃO
Departamento de Física, CFM-UFSC, CP 478, 88040-900 Florianópolis, SC, Brazil; joao@fsc.ufsc.br
TIMOTHY M. HECKMAN
Johns Hopkins University, Department of Physics and Astronomy, Baltimore, MD 21218; heckman@pha.jhu.edu
DANIEL J. LENNON
Isaac Newton Group, Apartado 321, 38700 Santa Cruz de La Palma, Canary Islands, Spain; djl@ing.iac.es
MAX PETTINI
Institute of Astronomy, University of Cambridge, Madingley Road, Cambridge CB3 0HA, England, United Kingdom; pettini@ast.cam.ac.uk
AND
CARMELLE ROBERT
Département de Physique, Université de Laval, Québec, QC G1K 7P4, Canada; carobert@phy.ulaval.ca
Received 2000 October 3; accepted 2000 November 28

ABSTRACT

We present synthetic ultraviolet spectra of metal-poor star-forming galaxies that were calculated with the Starburst99 package. A new spectral library was generated from *Hubble Space Telescope* observations of O stars in the Large and Small Magellanic Clouds. The corresponding mean metallicity of the synthetic spectra is approximately $\frac{1}{4}\ Z_\odot$. The spectra have a resolution of 1 Å and cover the spectral range 1200–1600 Å. A set of model spectra was calculated for a standard initial mass function and star formation history and is compared to synthetic spectra at solar metallicity. We find that the spectral lines are generally weaker at lower metallicity, as expected from the lower elemental abundances. Stellar wind lines, however, show a more complex behavior: the metallicity dependence of the ionization balance can be important in trace ions, like N^{4+} and Si^{3+}. Therefore, the strength of N V λ1240 and Si IV λ1400 does not scale monotonically with metallicity. We compare our new models to ultraviolet spectra of NGC 5253 and MS 1512-cB58, two star-forming galaxies with one-fourth solar metallicity at low and high redshifts, respectively. The new library provides significantly better fits to the observations than earlier models using the $Z_\odot$ library. We discuss the potential of utilizing stellar photospheric and wind lines to estimate the chemical composition of star-forming galaxies. The new metal-poor synthetic spectra are available via the Starburst99 Web site.

Subject headings: galaxies: starburst — galaxies: stellar content — stars: early-type — stars: mass loss — ultraviolet: galaxies

1. INTRODUCTION: STAR-FORMING GALAXIES IN THE ULTRAVIOLET

The ultraviolet (UV) to near-infrared (IR) line spectra of galaxies with current star formation exhibit a pronounced dichotomy: the UV region is dominated by strong stellar and interstellar *absorption* lines, whereas in the optical and near-IR such lines (if present at all) are hidden by strong interstellar *emission* lines (see Fig. 13 of Kinney et al. 1996). Therefore, the UV is the wavelength region of choice for the direct detection of stellar features in star-forming galaxies. The most extensive documentation of the UV spectral morphology of star-forming galaxies was published by Kinney et al. (1993), who compiled an atlas of all usable spectra in the *IUE* archive. More recently, the *Hubble Space Telescope*'s superior sensitivity and spatial as well as spectral resolution have made it possible to study a number of galaxies in much greater detail (Leitherer 2001).

The UV line spectra of local star-forming galaxies have become an important tool for the interpretation of the rest-frame UV of star-forming galaxies at high redshift (Conti, Leitherer, & Vacca 1996). The similarity of the spectra at low and high redshifts suggests similar stellar content (Ebbels et al. 1996; Steidel et al. 1996; Yee et al. 1996; Dey et al. 1997; Lowenthal et al. 1997; Pettini et al. 2000).

The underlying physics for the spectral appearance is rooted in the atmospheric conditions of hot, massive stars. Stars with masses upward of $\sim 10\ M_\odot$ and temperatures higher than $\sim$25,000 K provide the UV light in star-forming galaxies. Such stars have strong stellar winds with velocities up to 3000 km s^{-1}, leading to strong blueshifted absorption lines or even P Cygni–type profiles in the UV (Walborn, Nichols-Bohlin, & Panek 1985). The strongest lines are typically N V λ1240, Si IV λ1400, and C IV λ1550. Since the properties of hot, massive stars change rapidly over cosmological timescales, their line profiles in galaxy spectra do so as well and are useful as tracers of the massive stellar population. The promise of utilizing stellar absorption lines of Si IV λ1400 and C IV λ1550 to infer the massive-star content was first recognized by Sekiguchi & Anderson (1987a, 1987b), who related their *equivalent widths* to the stellar initial mass function (IMF). The relative strengths of these two lines can be used as a an indicator of massive stars

[1] Operated by AURA, Inc., under NASA contract NAS5-26555.

(e.g., Mas-Hesse & Kunth 1999) as well as of the kinematic conditions of the interstellar medium (Heckman et al. 1998).

The earlier *IUE* work using this diagnostic tool was limited to equivalent width determinations in galaxy spectra. With the *Hubble Space Telescope* (*HST*), UV *line profile* studies are feasible, and the full information of the profile shapes can be taken into account. This becomes particularly crucial for galaxies with strong interstellar lines whose interstellar and stellar wind components are often severely blended. Semiempirical UV spectral templates at 0.75 Å resolution were computed from evolutionary synthesis models by Robert, Leitherer, & Heckman (1993), Leitherer, Robert, & Heckman (1995), and de Mello, Leitherer, & Heckman (2000). These models linked a stellar UV library to the Starburst99 code (Leitherer et al. 1999) to produce a grid of UV line spectra for a standard set of stellar parameters. In many cases, the calculated spectra are in rather good agreement with observed galaxy spectra (e.g., Johnson et al. 1999; Pettini et al. 2000; Tremonti et al. 2001).

In our previous modeling, the spectral library used for the comparison with the galaxy spectra was built from hot stars with approximately solar or slightly subsolar chemical composition, although the galaxies were known to be more metal poor. Until recently, no library of metal-poor stars was available since *IUE*'s high-dispersion mode is required for adequate spectral resolution, and therefore only nearby bright OB stars could be observed. The stars of choice would be in the Magellanic Clouds where OB stars have metallicities lower by factors of 3–10 than their Galactic counterparts in the vicinity of the Sun (Garnett 1999). Observations of hot stars in the Large (LMC) and Small (SMC) Magellanic Clouds have been accumulated with *HST*'s UV spectrographs over several cycles in the past. These data are suitable for the construction of a low-metallicity UV library of hot stars as discussed in the preliminary work of Robert (1999a).

The purpose of this paper is to report the availability of a UV spectral library of LMC and SMC stars and to discuss its application to the study of the stellar content of star-forming galaxies with metallicities similar to those of the Magellanic Clouds. In § 2 we describe the data set and the reduction procedure. The generation of the library and its properties are discussed in § 3. In § 4, a series of synthetic low-metallicity spectra is presented. The synthetic spectra are compared to observations of NGC 5253 and MS 1512-cB58, two metal-poor galaxies at low and high redshifts, respectively (§ 5). Conclusions are given in § 6.

2. OBSERVATIONS AND DATA REDUCTION

2.1. *Sample Definition*

The library spectra were obtained with four *HST* General Observer (GO) programs between cycles 1 and 7: 2233 (PI: Kudritzki), 4110 (PI: Kudritzki; carryover program of 2233), 5444 (PI: Robert), and 7437 (PI: Lennon). Programs 5444 and 7437 had the specific science goals of creating a UV spectral library of LMC/SMC stars. The goal of programs 2233 and 4110 was to obtain spectra of hot stars for an atmospheric analysis; since the data are perfectly adequate for our intended library, they were included as well. We visually inspected the spectra of all targets in the four programs using the *HST* archive preview tool. Failed observations and spectra with very low signal-to-noise ratios (S/Ns) were discarded. Fifty-nine useful spectra were selected for a total of 53 stars, which are listed in Table 1.

The library stars in Table 1 are arranged by advancing spectral type. The sources for the identifiers are as follows: NGC 346 is an H II region in the SMC, and the star numbers are in the nomenclature by Massey, Parker, & Garmany (1989) and Walborn et al. (1995a). Note that Nos. 435, 355, 342, and 324 of Massey et al. (1989) are Nos. 1, 3, 4, and 6 of Walborn et al. (1995a), respectively. "Sk" stands for Sanduleak and denotes entries from Sanduleak's (1969) atlas of the LMC. "AV" entries are from the catalog of early-type SMC stars by Azzopardi & Vigneau (1975, 1982). The "BI" label was introduced by Crampton (1979) and refers to the LMC OB star catalog of Brunet et al. (1975). The identifiers in Table 1 are the same as used in the original *HST* programs in order to facilitate matching the spectra presented here with the original data, with these exceptions: Nos. 355 and 324 are called Nos. 3 and 6 in program 4110, all "Sk" stars in program 5444 are called "NS" (for Nick Sanduleak), and the declination zone and running index are inverted (e.g., Sk $-69°124$ becomes NS 124 -69).

The stellar spectral types (col. [3] of Table 1) are based on the classification work of Conti, Garmany, & Massey (1986), Garmany, Conti, & Massey (1987), Walborn et al. (1995a), and Walborn et al. (2000). Spectral coverage is complete from O3 through B0 if the whole LMC and SMC sample is considered, but significant spectral gaps are present for each galaxy sample individually. Therefore, we decided to build a mean library of LMC and SMC stars, with a corresponding mean metallicity of about $\frac{1}{4}\ Z_{\odot}$. We searched the *HST* archive for suitable spectra of stars with later spectral types, but none were found. The color excess $E(B-V)$ in column (4) of Table 1 was calculated from the observed and the intrinsic $B-V$. The photometry was taken from the same sources as the spectral types. The intrinsic color was assumed to be $B-V=-0.31$, independent of spectral type. The mean $E(B-V)$ of all 53 stars is 0.11.

2.2. *STIS Data*

A description of the technical aspects of the Space Telescope Imaging Spectrograph (STIS) data set was given by Walborn et al. (2000). The data were taken with the STIS FUV-MAMA detector in the E140M mode. The $0\farcs2 \times 0\farcs2$ entrance aperture was used. This instrument setup provides a 1 pixel resolving power of $R = 92{,}000$ over a wavelength range of 1150–1700 Å.

The data were retrieved from the *HST* archive and recalibrated with the IRAF/STSDAS software at STScI. The standard "calstis" calibration pipeline steps were followed, except for the one-dimensional spectrum extraction. The standard pipeline does not adequately correct for the underlying background due to scattered light. Therefore, a prototype version of the "x1d" package was used that corrects for scattered light with the algorithm of Howk & Sembach (2000). Tests with the black Milky Way Lyα absorption trough in the spectra demonstrated that this algorithm successfully accounted for the scattered light. After the individual orders were extracted, they were merged into a single spectrum with a beta version of the "splice" application within the "calstis" package. This application merges the orders with an optimized solution for the overlap region.

TABLE 1

LIBRARY STARS

Identifier (1)	Galaxy (2)	Spectral Type (3)	$E(B-V)$ (4)	Instrument (5)	*HST* Program (6)
NGC 346 No. 355.....	SMC	ON3 III(f*)	0.08	FOS, STIS	4110, 7437
Sk −66°172.....	LMC	O3 III(f*)	0.19	FOS	2233
Sk −68°137.....	LMC	O3 III(f*)	0.24	FOS	2233
AV 14.....	SMC	O3–4 V	0.12	FOS	5444
AV 388	SMC	O4 V	0.10	FOS	4110
NGC 346 No. 324.....	SMC	O4 V((f))	0.07	FOS, STIS	4110, 7437
Sk −70°60	LMC	O4 V	0.12	FOS	5444
NGC 346 No. 1	SMC	O4 III(n)(f)	0.11	FOS	4110
Sk −67°166.....	LMC	O4 If+	0.09	FOS	4110
NGC 346 No. 368.....	SMC	O4–5 V((f))	0.08	STIS	7437
AV 80.....	SMC	O4–6n(f)p	0.17	STIS	7437
AV 61.....	SMC	O5 V	0.07	FOS	5444
Sk −70°69	LMC	O5 V	0.06	FOS	2233, 5444
AV 75.....	SMC	O5 III(f+)	0.15	FOS, STIS	5444, 7437
NGC 346 No. 4	SMC	O5–6 V	0.08	FOS	4110
AV 243	SMC	O6 V	0.09	FOS	4110
AV 377	SMC	O6 V	0.00	FOS	5444
NGC 346 No. 113.....	SMC	OC6 V	0.09	STIS	7437
Sk −66°100.....	LMC	O6 II(f)	0.10	FOS	2233
HDE 269357.....	LMC	O6 I	0.10	FOS	5444
AV 220	SMC	O6.5f?p	0.09	STIS	7437
Sk −70°91	LMC	O6.5 V	0.08	FOS	5444
AV 15.....	SMC	O6.5 II(f)	0.09	FOS, STIS	5444, 7437
AV 207	SMC	O7 V	0.09	FOS	5444
BI 155	LMC	O7 V	0.11	FOS	5444
BI 208	LMC	O7 V	0.02	FOS	5444
AV 26.....	SMC	O7 III	0.13	FOS	5444
AV 95.....	SMC	O7 III((f))	0.01	STIS	7437
BI 229	LMC	O7 III	0.14	FOS	5444
BI 272	LMC	O7 II	0.16	FOS	5444
AV 83.....	SMC	O7 Iaf+	0.18	STIS	7437
AV 232	SMC	O7 Iaf+	0.10	FOS	4110
AV 69.....	SMC	OC7.5 III((f))	0.09	STIS	7437
AV 378	SMC	O8 V	0.07	FOS	5444
Sk −67°191.....	LMC	O8 V	0.10	FOS	5444
AV 47.....	SMC	O8 III((f))	0.05	FOS, STIS	5444, 7437
BI 9	LMC	O8 III	0.14	FOS	5444
BI 173	LMC	O8 III	0.17	FOS	5444
AV 469	SMC	O8 II	0.09	FOS	5444
AV 396	SMC	O9 V	0.08	FOS	5444
AV 451	SMC	O9 V	0.08	FOS	5444
AV 223	SMC	O9 III	0.11	FOS	5444
AV 238	SMC	O9 III	0.09	FOS	4110
Sk −67°101.....	LMC	O9 III	0.14	FOS	5444
Sk −69°124.....	LMC	O9 Ib	0.12	FOS	5444
AV 372	SMC	O9 I	0.13	FOS	5444
BI 192	LMC	O9.5 III	0.12	FOS	5444
BI 170	LMC	O9.5 II	0.14	FOS	5444
AV 327	SMC	O9.5 II–Ibw	0.09	STIS	7437
AV 170	SMC	O9.7 III	0.08	STIS	7437
Sk −65°21	LMC	O9.7 Iab	0.15	FOS	4110
NGC 346 No. 12.....	SMC	O9.5–B0 V	0.16	STIS	7437
AV 488	SMC	B0.5 Iaw	0.18	FOS	4110

Following the basic reduction, several additional reduction steps were applied. First, we co-added multiple exposures of the same stars. Then, we normalized the continuum to unity after division by a Chebyshev polynomial fitted to line-free sections of the spectrum. The continuum normalization process removed a flux depression between 1435 and 1440 Å due to shadowing by the STIS MAMA repeller wire. The effect on the spectrum is a lower S/N in this wavelength region. Next, a velocity offset of -150 km s^{-1} was added to account for the recession velocity of the SMC (all LMC stars were observed with the Faint Object Spectrograph [FOS]). Finally, the spectra were resampled and truncated to match the spectral resolution and wavelength coverage of the spectra obtained with the FOS. The sampling and spectral resolution were decreased to 0.75 Å $pixel^{-1}$. The starting wavelength was set to 1205.5 Å, which

is the same as that of the $Z_\odot$ library. The spectra were truncated at 1601 Å, since the FOS data terminate at that wavelength.

The final reduced spectra are essentially identical to those of Walborn et al. (2000), which were processed with an independent algorithm.

2.3. *FOS Snapshot Data*

The FOS Snapshot spectra of program 5444 were taken with the blue FOS detector through the $1\farcs2 \times 3\farcs7$ entrance aperture. The target acquisition mode was "point and shoot"; i.e., the spectra were taken without additional centering after the initial guide-star acquisition. Due to the large aperture used and the expected pointing error of 1″–2″, most (but not all) observations succeeded, and well-exposed spectrograms are in the *HST* archive. Each star was observed with two gratings, G130H and G190H, resulting in a wavelength coverage of 1140–1605 Å and 1573–2330 Å, respectively. The nominal spectral resolution for a point source observed with G130H is 1.0 Å. Since the STIS spectral coverage ends at 1700 Å, the same maximum wavelength should apply to the FOS data as well. We decided not to include the G190H spectra in the library because (1) the extra $\sim$100 Å would not add other strong stellar lines in a galaxy spectrum and (2) the 1600–1700 Å region is at the sensitivity boundaries for both gratings, with low count numbers and large calibration uncertainties. Unfortunately, the (generally weak) He II λ1640 line is longward of this cutoff and cannot be synthesized.

The retrieved spectra were processed with the "calfos" pipeline within IRAF/STSDAS. The processed spectra were not significantly different from the calibrated spectra in the archive. Several spectra showed spurious emission lines around 1430 and 1510 Å. In all cases they turned out to be artifacts due to intermittent diodes. The features were successfully removed by interpolation between the adjacent continuum. The subsequent data processing was similar to that applied to the STIS data. Multiple exposures were co-added, the continuum was normalized to unity, and radial velocity corrections of -150 and -270 km s^{-1} were added to the SMC and LMC data, respectively. Most spectra showed significant wavelength offsets even after the radial velocity correction. This was expected since the point-and-shoot target acquisition can place the star anywhere inside (and sometimes outside) the $1\farcs2 \times 3\farcs7$ aperture, which extends over four science diodes. Therefore, wavelength shifts of ± 2 Å can occur. The shifts were corrected by establishing a wavelength zero point with strong interstellar lines in the STIS spectra and then determining the offset in the FOS data.

The final step was to resample the spectra to 0.75 Å pixel^{-1} and to truncate them at the same boundaries as the STIS data. A value of 0.75 Å is slightly higher but still close to the nominal spectral resolution of 1.0 Å.

2.4. *FOS GO Data*

The observations from GO programs 2233 and 4110 were performed prior to the installation of Costar. As in the Snapshot program, G130H and G190H spectra were taken. Since the data were obtained in the aberrated beam, the narrow $0\farcs25 \times 2\farcs0$ entrance slit was used to retain the full nominal spectral resolution. A full target acquisition, including peak-ups, was required to center the star.

As we did with the Snapshot data, only the G130H spectra were considered. All reduction steps were analogous to the Snapshot processing. Although these spectra did not suffer from the large wavelength offsets due to a missing target acquisition, we nevertheless found that the standard FOS wavelength calibration could be improved by comparing them to the STIS data. Therefore, we determined and applied the wavelength offsets in the same way as we did for the Snapshot data. The final product was a wavelength-calibrated, normalized spectrum from 1205.5 to 1601 Å at 0.75 Å sampling for each star.

We co-added the spectra of six stars with data from more than one program: NGC 346 No. 355, NGC 346 No. 324, Sk $-70°69$, AV 75, AV 15, and AV 47. This then resulted in a total of 53 unique stellar templates with typical S/Ns of about 30 (as determined mostly by the FOS data; the STIS spectra have higher S/Ns).

3. GENERATION OF THE LIBRARY

The low-metallicity library was built with the same rules that we used for the solar metallicity library in Starburst99 (Robert et al. 1993; de Mello et al. 2000). We averaged the spectra of stars with the same spectral type in order to increase the S/N and to minimize the impact of spectral misclassifications. Although only stars with classifications based on slit spectra are considered, the spectral types of some stars are less certain due to the quality of the optical classification spectra. The format of the library is a two-dimensional grid with 15 temperature classes between O3, O3.5, O4, O4.5, ..., B0 and five luminosity classes of V, IV, III, II, and I. This grid is dictated by the interpolation scheme in Starburst99 and does not directly correspond to the MK classification grid of O stars. The spectral types in Table 1 were sufficient to populate about 40% of this grid. Missing entries (mostly stars with luminosity classes IV and II) were filled by two-dimensional interpolation between adjacent temperature and luminosity classes.

The conversion from spectral type to temperature and luminosity is done with the prescription of Schmidt-Kaler (1982). This relation is somewhat different for O stars than that of Vacca, Garmany, & Shull (1996). As a test, we selected the subset of 15 SMC O stars discussed by Walborn et al. (2000) and placed them on a Hertzsprung-Russell diagram using both our calibration and that of Vacca et al. The mean temperature and log bolometric luminosity differences (Schmidt-Kaler–Vacca) are -2100 ± 800 K and 0.03 ± 0.12, respectively. The average temperature shift is smaller than 5% and corresponds to less than one spectral subtype. These are the uncertainties that should be kept in mind when reconstructing a Hertzsprung-Russell diagram with our method. Clearly, the stellar positions on such a diagram predicted by Starburst99 have larger errors than those derived via a dedicated atmospheric analysis. In addition, if the temperature and luminosity scales of Schmidt-Kaler needed significant revision, the assignment of library spectra to positions in the Hertzsprung-Russell diagram would be modified as well. In our opinion, there is no clear evidence for substantial flaws in either the Schmidt-Kaler or the Vacca et al. scales, and the differences simply reflect current uncertainties in hot-star models.

In Figures 1–4 we show examples of four spectral groups with types O4 V, O9 V, O4 I, and O9 I. The four groups are representative of the temperature and luminosity behavior of the strongest strategic lines of N V λ1240, Si IV λ1400, and

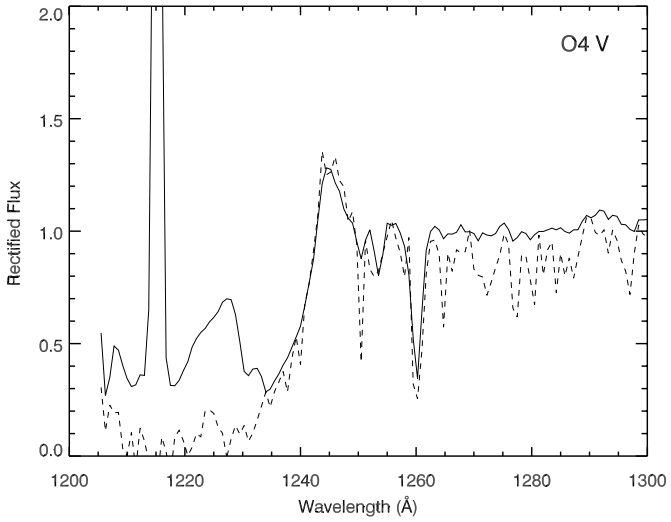

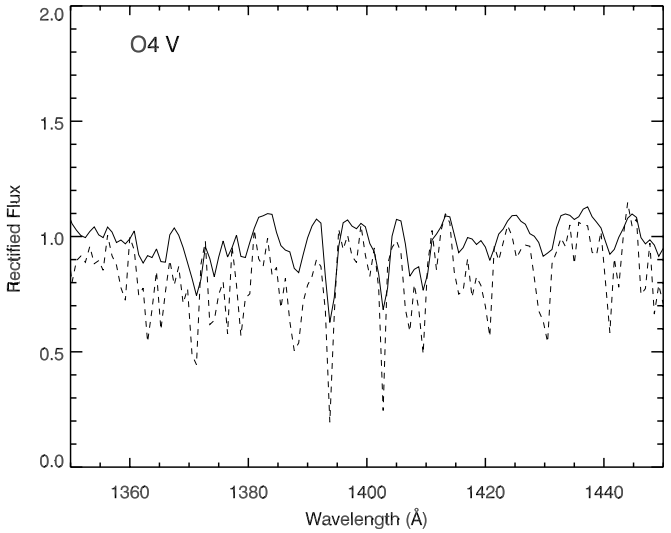

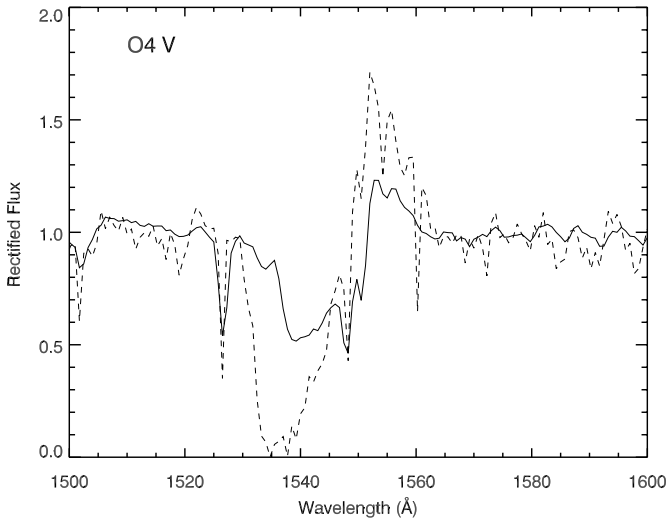

FIG. 1.—Comparison between the low (*solid lines*) and solar metallicity (*dashed lines*) spectra within the O4 V spectral group. *Top*: N V λ1240; *middle*: Si IV λ1400; *bottom*: C IV λ1550.

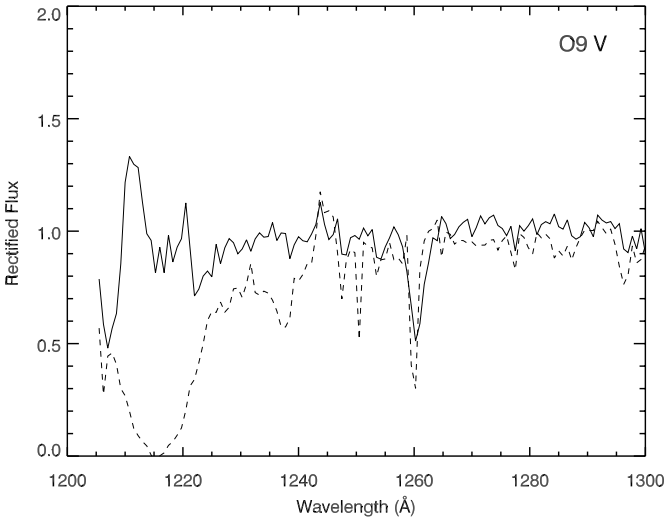

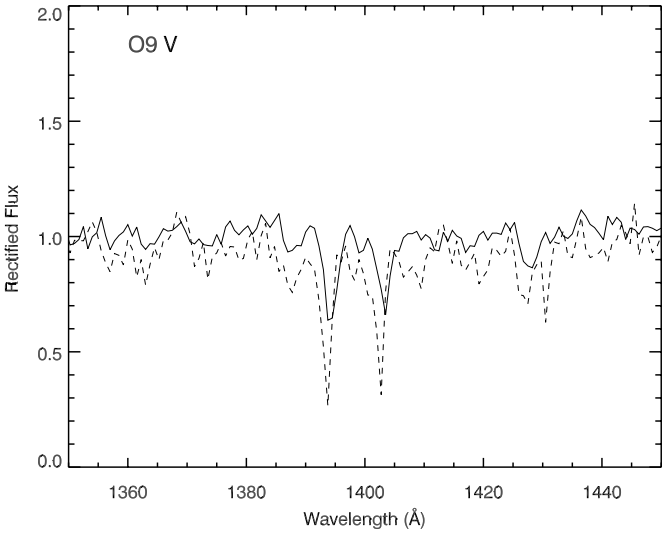

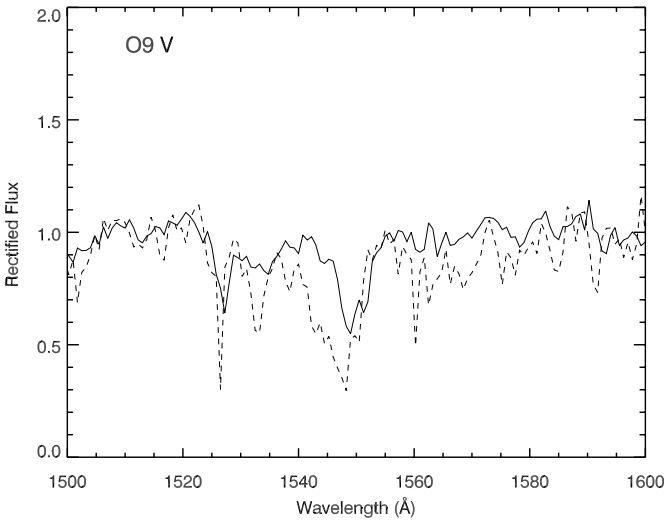

FIG. 2.—Same as Fig. 1 but for spectral group O9 V

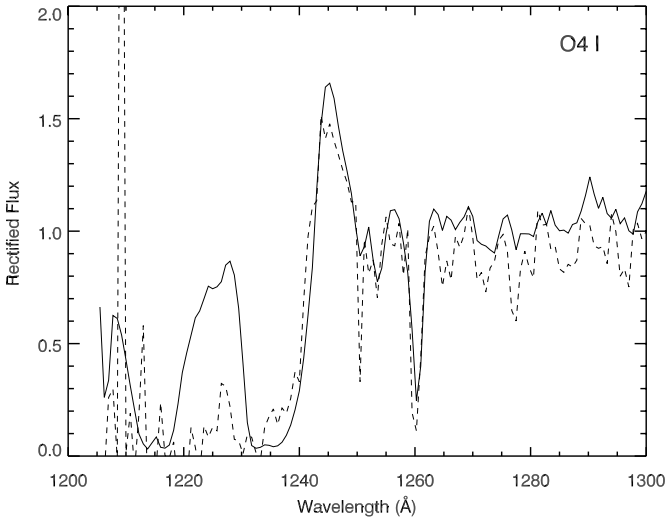

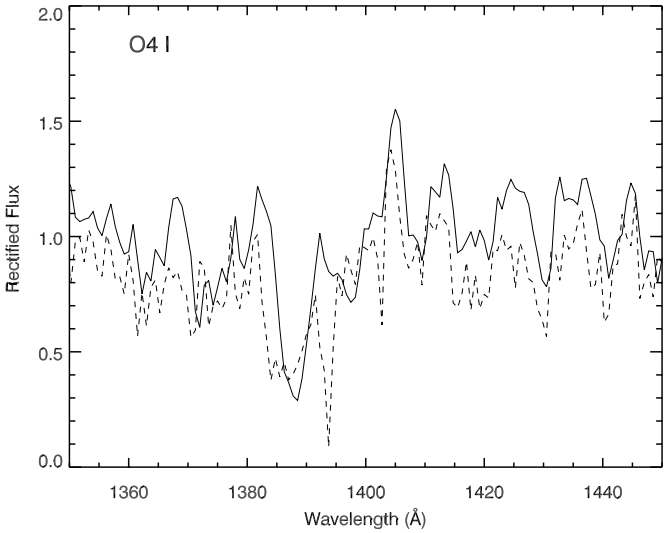

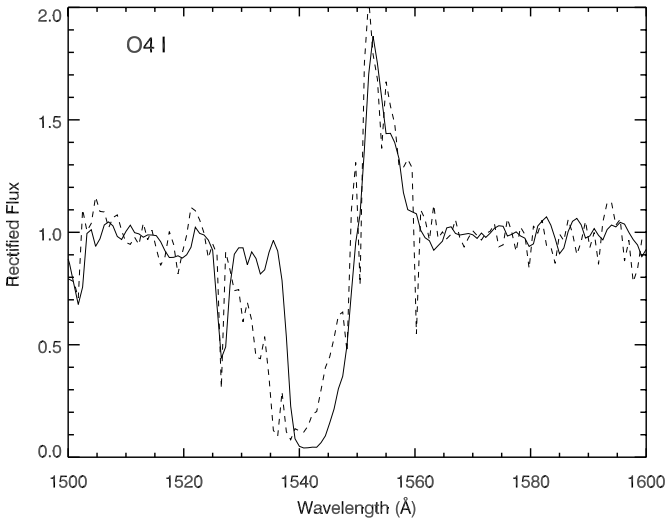

FIG. 3.—Same as Fig. 1 but for spectral group O4 I

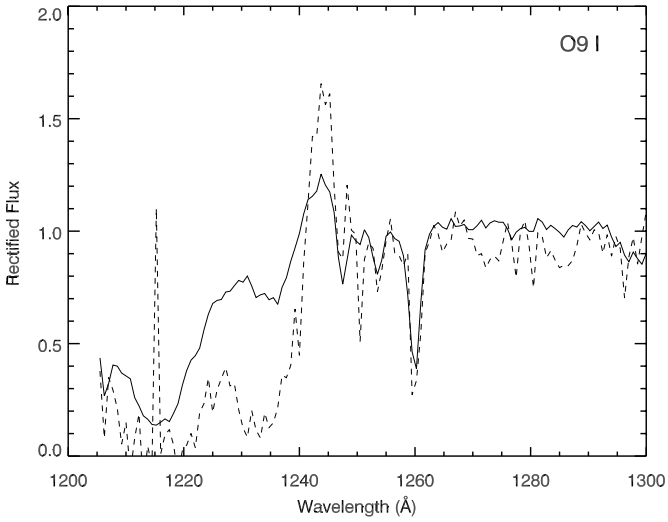

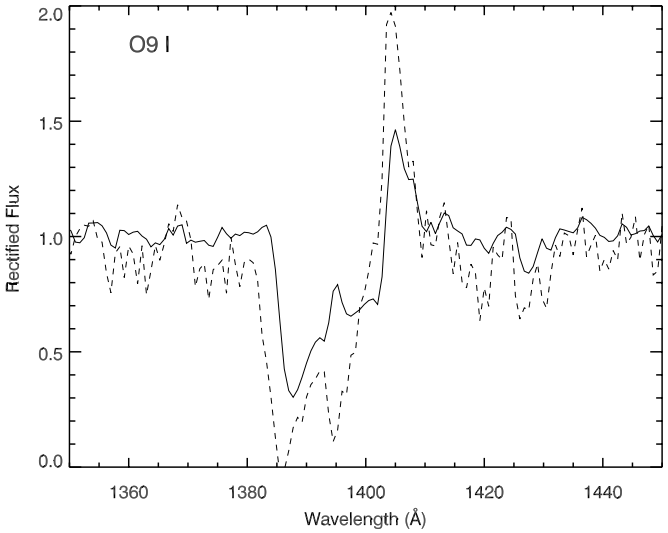

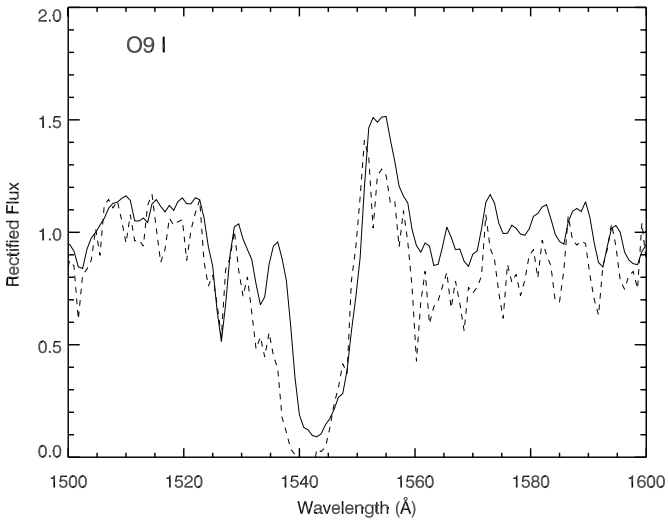

FIG. 4.—Same as Fig. 1 but for spectral group O9 I

C IV λ1550. A discussion of the properties of these lines at solar metallicity was given in Leitherer et al. (1995). The corresponding spectral groups at $Z_\odot$ are included in Figures 1–4 for comparison. As expected, the spectral features are generally (but not always) weaker at lower metallicity (see the discussion by Robert 1996, 1999b and Plante 1998). Photospheric lines are uniformly weaker in the low-metallicity library due to the lower opacity in the Magellanic Clouds (Haser et al. 1998). Stellar wind lines are more complex, as both metallicity and wind properties determine their opacities. Under most wind conditions, N^{4+}, Si^{3+}, and C^{3+} are trace ions (Lamers et al. 1999), so slight changes in the stellar temperature can increase or decrease the line strengths significantly.

Early O main-sequence stars (Fig. 1) display wind effects in N V λ1240 and C IV λ1550 but not in Si IV λ1400. This was first noted by Walborn & Panek (1984) and explained as an ionization effect of Si^{3+} in main-sequence stars with less dense winds by Drew (1990) and Pauldrach et al. (1990). The Si IV doublet absorption in *any* O main-sequence star is almost exclusively interstellar. N V λ1240 has no significant metallicity dependence in the O4 V group. (The N V profile shortward of 1230 Å is blended with interstellar and geocoronal Lyα.) The behavior of the N V λ1240 line is a prime example of the counteracting effects of chemical composition and stellar temperature on the N^{4+} column density. The dominant ionization stage in O star winds is N^{3+}, and the mean ionization fraction of N^{4+} increases monotonically with stellar temperature (Lamers et al. 1999). Therefore, to first order, the N^{4+} becomes independent of the stellar mass loss because the ionization fraction and the total nitrogen column density ($=\sum N^i$) have the opposite dependence on $\dot{M}$. Full non-LTE model atmosphere calculations by Kudritzki (1998; his Fig. 7) agree with this plausibility argument: the N V λ1240 line is stronger in models at $Z = \frac{1}{5} Z_\odot$ than at $Z_\odot$. In contrast to N V λ1240, C IV λ1550 is much weaker and the absorption is less blueshifted at lower metallicity, a direct result of the lower wind density and velocity in the Magellanic Clouds. Ionization effects are less important for C^{3+}, so the column density of the C^{3+} ion scales with the total column density of carbon.

The same trends are present in late O main-sequence stars (Fig. 2). The wind effects are dramatically reduced for O9 V stars due to their much lower luminosity. The only indication of a stellar wind at low metallicity is the asymmetric C IV λ1550 profile. At solar metallicity, this line becomes blueshifted due to the increased wind opacity.

Stellar mass loss increases with luminosity as $\dot{M} \propto L^{1.5}$ (Garmany & Conti 1984), and wind velocities are proportional to the surface escape velocity: $v_\infty \propto v_{\rm esc}$ (Lamers, Snow, & Lindholm 1995). Therefore, the wind densities increase by an order of magnitude from luminosity class V to I for the same spectral type. N V λ1240, Si IV λ1400, and C IV λ1550 have strong P Cygni profiles over most of the O supergiant spectral sequence due to the enhanced wind opacity. Both early O (Fig. 3) and late O (Fig. 4) supergiants in the Magellanic Clouds and in the Galaxy have similar profiles, suggesting that metallicity becomes less important for more saturated line profiles, in comparison with the (mostly) optically thin profiles of main-sequence stars. There is, however, a clear indication of the lower metallicity of the Magellanic Cloud stars from the wavelength displacement of the absorption component: low-metallicity stars always have a smaller extent (i.e., terminal velocity) than their Galactic counterparts.

4. SYNTHETIC GALAXY SPECTRA

The 75 spectral groups (15 temperature and 5 luminosity classes) were used to replace the existing solar metallicity groups of type O in Starburst99. All other spectral groups are still at the original (near) solar metallicity.[2] This can affect the computed synthetic spectra of an evolving population, depending on the IMF and/or the age. The validity range of the low-metallicity library can be easily assessed: since the lifetime of the least massive O stars is ∼10 Myr (Schaller et al. 1992), the UV spectrum of a *single* stellar population with a standard Salpeter IMF up to 100 $M_\odot$ will be determined by the LMC/SMC stars until about 10 Myr. Later on, the original Galactic B stars will produce the spectrum.

If stars form *continuously*, a near equilibrium of the UV light is reached after about 10 Myr. In this case, the synthetic UV spectrum is a mix of the new LMC/SMC stars and the original Galactic stars, and the consequences of omitting low-metallicity B stars are not immediately obvious. In general, the stellar wind lines, such as N V λ1240, Si IV λ1400, or C IV λ1550, are from massive (>40 $M_\odot$) stars. Therefore, the profiles of these lines predicted by a synthetic model will still be correct for all the ages considered if B supergiants (the descendants of massive main-sequence stars) can be neglected. On the other hand, the continuum and many photospheric lines are due to less massive B stars, for which we use the solar metallicity library. These lines would be too strong in our models if compared to observations of metal-poor galaxies for which a continuous model with age older than 10 Myr is deemed appropriate. We performed the following test: the rectified solar metallicity B stars in the library with temperatures below 25,000 K were replaced by a line-free continuum. This simulates the extreme assumption of zero-metallicity B stars. The O and early B (until B0.5) spectra were left unchanged, i.e., with the LMC/SMC stars. In Figure 5 we compare two spectra computed with this artificial library and with the new LMC/SMC O star and Galactic B star

[2] Note that the existing "solar" metallicity library is actually somewhat subsolar since the Sun has a metal overabundance of ∼0.2 dex (Smartt & Rolleston 1997) with respect to nearby H II regions where the library stars are located. For simplicity, we refer to the existing library as "solar metallicity."

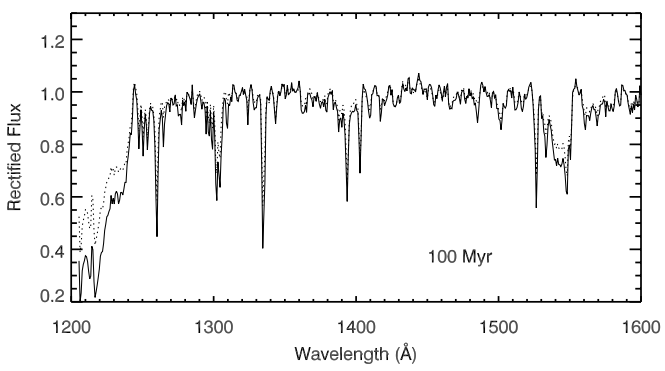

FIG. 5.—Comparison between a model spectrum at $\frac{1}{4} Z_\odot$ computed with the new library (*solid line*) and with an artificial library having line-free B star spectra (*dotted line*). Continuous star formation, Salpeter IMF with $M_{\rm low} = 1\ M_\odot$ and $M_{\rm up} = 100\ M_\odot$, age 100 Myr.

library. Both spectra are for continuous star formation at age 100 Myr and with a Salpeter IMF. Despite the extreme assumption for the B star spectra, the differences are not dramatic. The wind profiles have somewhat weaker absorptions. This results from adding a featureless continuum in this test, whereas in reality even an LMC/SMC B star would have some absorption, producing stronger wind lines in the synthetic spectrum. The outcome of this test depends quite sensitively on the cutoff temperature for the replaced B stars. Choosing 30,000 K instead of 25,000 K would affect the lines of, e.g., Si III λ1417 and C III λ1427, whose strength is heavily weighted towards the earliest B stars with temperatures between 25,000 and 30,000 K. We conclude that omission of LMC/SMC stars later than B1 does not affect the interpretation of the star formation histories presented in this paper.

The absolute flux levels of the continuum are always treated correctly since evolutionary tracks and model atmospheres with the appropriate chemical composition are used. Therefore, the above limitations do not apply.

Details of the input physics and computation technique in Starburst99 are given in Leitherer et al. (1999). We computed a set of standard model spectra for evolving starbursts with and without ongoing star formation. The former and the latter will be referred to as the "instantaneous" and the "continuous" cases, respectively. A standard Salpeter IMF with slope $\alpha = 2.35$ between 1 and 100 $M_\odot$ and stellar evolution models with a metallicity of $\frac{1}{5}\,Z_\odot$ are used.

A time series for an instantaneous starburst between 0 and 10 Myr is shown in Figure 6. The spectra discussed in this paper are normalized to the unity level. All spectra were computed in luminosity units as well to permit estimates of, e.g., the dust obscuration and the star formation rates. The corresponding luminosities are not reproduced here as they are the same as in Figure 53*d* of Leitherer et al. (1999). Both the normalized and the absolute luminosities are part of the output of Starburst99 and can be retrieved from the Web site given at the end of this paper. The line profiles have the same qualitative behavior as in the solar metallicity models discussed by Leitherer et al. (1995). They gradually strengthen from a main-sequence–dominated population at 0–1 Myr to a population with luminous O supergiants at 3–5 Myr. Afterward, the emission components decrease until the line spectrum is due to a population of early B stars at 10 Myr. At that time, the spectrum in Figure 6 starts showing contributions from solar metallicity stars. Si IV λ1400 is strongest at 4–5 Myr. This is different from the solar metallicity case, where this line reaches its maximum at 3–4 Myr (see Fig. 6 of Leitherer et al. 1995). The reason is stellar evolution, not the difference in the library spectra. Stars with lower metallicity have longer main-sequence lifetimes and are hotter. Therefore, the entrance into the phase when Si IV λ1400 becomes strong is delayed with respect to the solar metallicity case. We verified this interpretation by computing a spectral sequence for the low-Z library with solar metallicity tracks. In this case, the peak strength of the Si IV profile is reached at about 4 Myr, similar to models with $Z_\odot$ library stars.

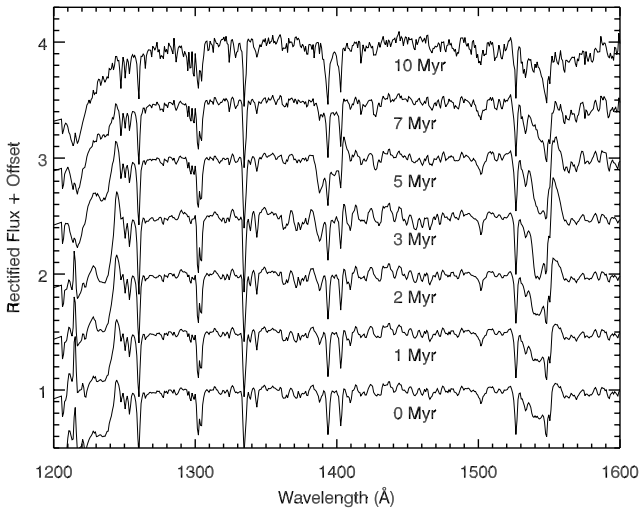

FIG. 6.—Evolution of a synthetic UV spectrum between 0 and 10 Myr. Parameters: instantaneous starburst, $\frac{1}{4}\,Z_\odot$, Salpeter IMF with $M_{\rm low} = 1\,M_\odot$ and $M_{\rm up} = 100\,M_\odot$.

How different are the new models from the earlier solar Z spectra? In Figure 7 (*top*) we compare the spectral region between 1200 and 1600 Å at $\frac{1}{4}\,Z_\odot$ and $Z_\odot$. At $t = 0$ Myr, for a zero-age main-sequence population, most photospheric and wind lines are significantly weaker at low metallicity than at $Z_\odot$. The wind profile of C IV λ1550 has both weaker emission and absorption, an immediate consequence of the lower mass-loss rates at lower Z. N V λ1240 remains essentially unchanged. Si IV λ1400 is purely interstellar, and the difference between the two spectra results from the different strengths of the interstellar lines in the library stars. Almost all weak *photospheric* lines from O stars scale with metallicity. The strong S V λ1502 is a notable exception: there is little change with metallicity. Most weak features can be seen at both metallicities. Since the two sets of library stars were acquired with different telescopes, they cannot be due to detector noise but are real stellar lines (Nemry, Surdej, & Herniaz 1991).

The majority of the weak photospheric lines are due to transitions in highly ionized iron and nickel (Haser et al. 1998). They have typical line widths of tens of kilometers per second resulting from microturbulent velocities of $\sim$20 km s^{-1} and stellar rotation velocities of $v \sin i$ between 0 and 100 km s^{-1}. Therefore, all unblended photospheric lines are unresolved in our library spectra. The comparison in Figure 7 demonstrates that all photospheric lines become weaker at lower metallicity. Most lines are too weak to be used as metallicity indicators individually, but the overall blanketing effect as a function of metallicity can provide a useful estimate of the chemical composition of a galaxy spectrum. The strongest photospheric lines showing a metallicity dependence are the Si III, C III, and Fe V blends around 1425 Å. In the next section, we will utilize these lines to estimate the chemical composition of the high-redshift galaxy MS 1512-cB58.

The 0 Myr–old population is a somewhat academic case since a genuine zero-age main-sequence population will hardly be observed in the UV; $t = 4$ Myr is more realistic (Fig. 7, *middle*). At that age, supergiants dominate, and the stellar wind profiles of N V λ1240, Si IV λ1400, and C IV λ1550 are at maximum strength. There is a mild metallicity dependence in the sense that the velocities are lower and the absorptions are weaker at lower Z. Overall, the effect is not very dramatic, as expected from the discussion of the individual stellar spectra in § 3. Since most star formation regions are observed when supergiants are present, our

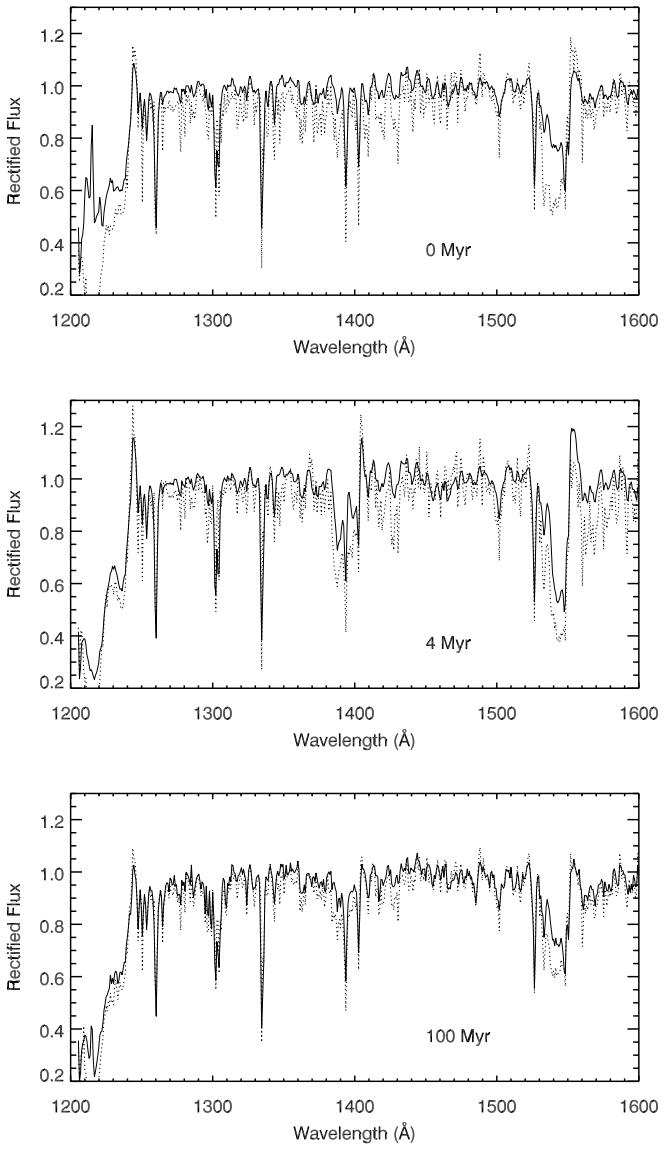

FIG. 7.—Comparison of three synthetic spectra at 0 Myr (*top*), 4 Myr (*middle*), and 100 Myr (*bottom*). *Solid lines*: $Z = \frac{1}{4}\ Z_\odot$; *dotted lines*: $Z = Z_\odot$. Salpeter IMF between 1 and 100 $M_\odot$; instantaneous starburst for the 0 and 4 Myr models and continuous star formation for the 100 Myr model.

models predict that *the stellar wind profiles become moderately weaker toward lower metallicity*. The metallicity trends of the photospheric lines are the same at 0 and 4 Myr, suggesting that age effects are less important.

The bottom panel of Figure 7 shows a comparison between $\frac{1}{4}\ Z_\odot$ and $Z_\odot$ models for continuous star formation at an age of 100 Myr. The most striking differences between the two spectra are the decreased photospheric line blanketing at lower metallicity and the weaker absorption component of the C IV λ1550 wind line. The N V and Si IV wind absorptions are rather similar, and the emission components of N V, Si IV, and C IV are essentially identical. The strongest photospheric lines from O and early B stars are O V λ1371, Fe V $\lambda\lambda$1360–1380, Si III λ1417, C III λ1427, and Fe V λ1430. Other relatively strong and unblended photospheric lines in a starburst spectrum are Si II λ1265 and λ1533. However, these lines are not very useful for our purpose of investigating metallicity effects since they arise from mid to late B stars, which are not included in our low-Z library. In contrast, the former lines around 1370 and 1425 Å do not suffer from this shortcoming.

We define line indexes "1370" and "1425" as the equivalent widths integrated between 1360 and 1380 Å and between 1415 and 1435 Å, respectively. These two indexes measure the metallicity-sensitive spectral blends from O and early B stars discussed above. They are plotted in Figure 8 for constant star formation models with Salpeter IMF between 1 and 100 $M_\odot$. Their weak age dependence and relatively strong sensitivity to the line blanketing makes them useful indicators of the metallicity. The metallicity dependence in Figure 8 is caused by two effects: the spectral features are weaker in metal-poor individual stars, *and* stellar evolution models are metallicity dependent as well. In addition, systematic errors in the models are not entirely negligible. The continuum normalization and the definition of the library star grid may have metallicity-dependent biases. For these reasons, the prudent approach would be to compare the actual spectrum over a larger wavelength range to the observations, rather than limiting the available information by measuring equivalent widths only. We estimate the *systematic* uncertainty of each point in Figure 8 to be about ± 0.1 Å, with a possible time dependence. Therefore, any trend with time is not significant.

In addition, there will be a possibly even larger error due to the adopted continuum location. This error is hard to quantify. Therefore, it is important to understand how the continuum is defined. Evolutionary synthesis is driven by stellar evolution models and their predicted dependence of stellar effective temperatures and bolometric luminosities with time. The emergent fluxes at any wavelength point come from model atmospheres. Therefore, our definition of the continuum is identical to that used in the model atmospheres. Since theoretical atmospheres know a priori the amount of line-blanketing at each wavelength point, the continuum is not derived by just fitting an unbiased power law to the fluxes. Rather, we first select wavelength intervals that are line free according to the atmosphere models. The wavelength points for the fits are 1150, 1280, 1310, 1360,

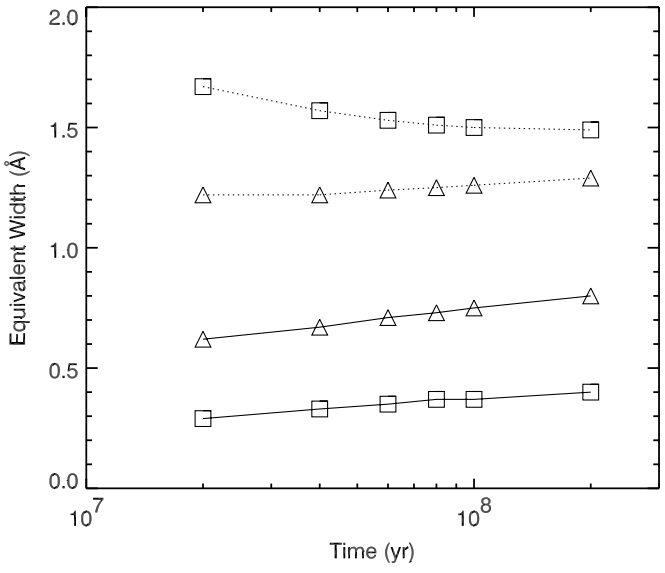

FIG. 8.—Equivalent width of the 1425 index (*squares*) and the 1370 index (*triangles*) vs. time. The symbols are connected by solid and dotted lines for $\frac{1}{4}\ Z_\odot$ and $Z_\odot$ metallicities, respectively. Continuous star formation with Salpeter IMF between 1 and 100 $M_\odot$.

1430, 1480, 1510, 1580, 1630, 1680, 1740, 1785, 1820, and 1875 Å. This is done for every single position in the Hertzsprung-Russell diagram. These wavelength regions are assumed to be pure continuum and to be time independent. This assumption is true for most of the time. If weak photospheric lines affect the chosen continuum points at certain time steps, the predicted continuum of the synthetic spectrum may be slightly offset from the unity level. Then, we fit a smooth curve through these points and replace the original model atmosphere by the smooth curve. Equivalently, one can describe this as removing any spectral lines and generating a "pseudoatmosphere" at an optical depth where free-bound, free-free, and e^--scattering processes dominate. The second step is to link the normalized, *line-blanketed* library spectra to the luminosity-calibrated *line-free* model atmospheres. The library spectra were rectified using the same prescription; i.e., we fitted a curve only to those spectral regions that we knew a priori are line free. This method is different from, e.g., the prescription in Walborn et al. (1985), who rectified the continuum to unity based on the empirical absence of features in a spectral region rather than the theoretical prediction of line blanketing. To summarize, the continuum level in the model spectra depends (1) on the fitting points of the pseudoatmosphere and (2) on the adopted normalization of the library spectra. The two-step approach is required due to the reddening of the model spectra. In the absence of reddening, we could have simply linked the luminosity-calibrated library spectra with stellar evolution models. It is crucial to recall these steps when comparing weak lines between models and observations. The continuum definition is a major source of uncertainty both in the observations and in the synthetic models.

Spectra of low-metallicity populations with continuous star formation from 0 to 500 Myr are shown in Figure 9. The properties of this sequence hold no surprises, given what was discussed before. Spectra with continuous star formation are relevant for the modeling of the integrated light of galaxies, such as, e.g., Lyman break galaxies at high redshift. For star formation timescales larger than about 50 Myr, only the C IV λ1550 stellar wind line can be readily recognized as stellar; all other stellar lines are blended with interstellar absorption lines. Apart from C IV λ1550, the next strongest stellar features are N V λ1240, Si IV λ1400, and the Si II and Si III multiplets around 1300 Å (see de Mello et al. 2000). Sufficiently high spectral resolution is required observationally in order to separate these features from interstellar Lyα, Si IV λ1400, and O I + Si II λ1303. Other stellar photospheric lines seen in these spectra are Si III λ1417, C III λ1427, and S V λ1502.

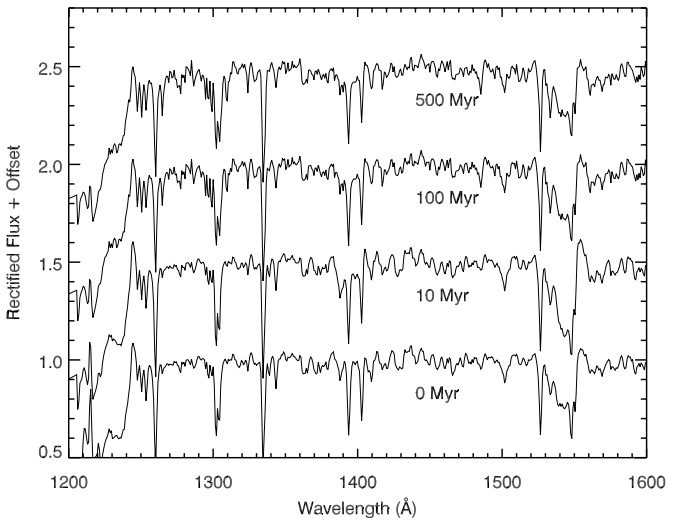

FIG. 9.—Evolution of a synthetic UV spectrum between 0 and 500 Myr. Parameters: continuous star formation, $\frac{1}{4}\,Z_\odot$, Salpeter IMF with $M_{\rm low} = 1\,M_\odot$ and $M_{\rm up} = 100\,M_\odot$.

5. COMPARISON WITH THE UV SPECTRA OF NGC 5253 AND MS 1512-cB58

The first application of the new low-metallicity library to UV observations of a star-forming galaxy was done by Tremonti et al. (2001) in their study of the metal-poor galaxy NGC 5253. This galaxy hosts numerous young super star clusters with an oxygen abundance of about $\frac{1}{6}\,Z_\odot$ (Calzetti et al. 1997). Since the analysis of the UV spectra was performed by Tremonti et al., we will not repeat their study but rather use their results to highlight the properties of the low-metallicity synthesis models.

In Figure 10 we compare the average spectrum of eight clusters in NGC 5253 to synthetic models at solar and one-fourth solar metallicity. The two models have the same parameters, except for the metallicity. The metallicity adopted in the evolutionary tracks is $Z_\odot$ and $\frac{1}{5}\,Z_\odot$ for the solar and the LMC/SMC library, respectively. A standard Salpeter IMF between 1 and 100 $M_\odot$ was used. The starburst is extended, with stars forming continuously for 6 Myr. This star formation history is appropriate for a superposition of eight clusters with ages between 1 and 7 Myr. However, the precise age does not strongly affect the computed spectrum for the case of continuous star formation (see Fig. 4 of Leitherer et al. 1995). The agreement between the average cluster spectrum and the modeled low-Z spectrum is excellent. The stellar wind features N V λ1240, Si IV λ1400, and C IV λ1550 are reproduced extremely well, except for the narrow interstellar contributions. We do not expect to match the interstellar lines in the observed spectrum for two reasons. First, the library stars have a mean reddening of $E(B-V) = 0.11$, whereas the cluster reddening is $\sim$0.25. Consequently, the column density of the interstellar lines in NGC 5253 is higher than in the LMC/SMC library stars, and the line strengths of not too deeply satu-

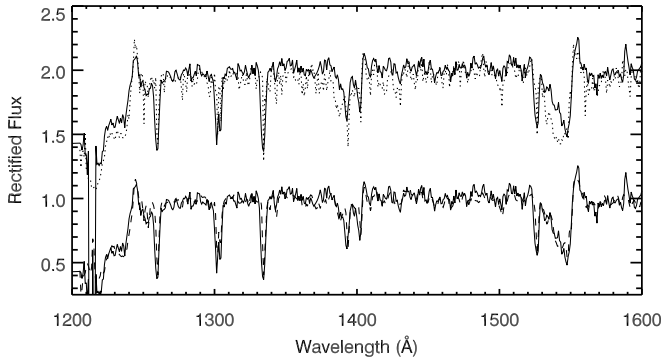

FIG. 10.—Comparison between the average spectrum of eight starburst clusters in NGC 5253 (*solid lines*) and two synthetic models at $Z = \frac{1}{4}\,Z_\odot$ (*lower; dashed line*) and $Z = Z_\odot$ (*upper; dotted line*). The models have continuous star formation, age 6 Myr, and Salpeter IMF between 1 and 100 $M_\odot$.

rated lines should be larger in NGC 5253. Second, and more important, Heckman & Leitherer (1997) suggested that the interstellar lines in NGC 1705 are broadened due to macroturbulence and blending of multiple components due the energy input from stellar winds and supernovae in starbursts. Generally, the interstellar medium in starburst galaxies is more turbulent than in the Milky Way and the Magellanic Clouds, so even saturated lines are stronger in starbursts.

The corresponding stellar wind lines produced by the $Z_\odot$ model spectrum are a worse fit to the observations. Particularly discrepant are the blue absorption wings in Si IV λ1400 and C IV λ1550, which are much too strong in the models. Reducing the number of the most massive stars with a steeper IMF would somewhat alleviate the problem, but at the price of a worse fit to the emission components. The ratio of the absorption to the emission strengths is therefore a sensitive indicator of the metallicity. We expect this relation to be tighter for C IV λ1550 than for N V λ1240 and Si IV λ1400 due to the previously discussed ionization effect. As opposed to C^{3+}, N^{4+} and Si^{3+} are trace ions in hot star winds, and changes in the ionization balance with metallicity complicate the direct metallicity dependence.

Photospheric line blanketing can be seen over the entire spectral range plotted in Figure 10. The most prominent examples are C III λ1428 and S V λ1502. Most photospheric lines are weak in comparison with wind lines, so metallicity effects are strong. Obviously, the low-metallicity spectrum provides a much better fit to the observations than the $Z_\odot$ model. The agreement between the modeled and observed photospheric lines suggests that the metallicity used in the model is appropriate for NGC 5253. Vice versa, the photospheric lines (and of course the C IV λ1550 wind profile) can be used *to determine the metallicity* if the other stellar properties are known independently.

As a second test, we apply our low-metallicity library to the rest-frame UV spectrum of the $z = 2.72$ galaxy MS 1512-cB58. This object was originally discovered in the CNOC cluster redshift survey by Yee et al. (1996) and subsequently found to be a lensed star-forming galaxy (Seitz et al. 1998). Its star formation history and general properties were explored by Ellingson et al. (1996), de Mello et al. (2000), Pettini et al. (2000), and Teplitz et al. (2000). Both de Mello et al. and Pettini et al. modeled the rest-frame UV spectrum of MS 1512-cB58 with the original $Z_\odot$ library in Starburst99. The new low-Z library allows us to model the UV spectrum in a truly self-consistent way.

The chemical composition of MS 1512-cB58 is known only approximately. Due to its redshift, a traditional emission-line analysis is not feasible since some of the key diagnostic lines, like [O III] λ4363, are inaccessible from the ground and/or are simply too faint to be observed. Nevertheless, Teplitz et al. (2000) were able to estimate an oxygen abundance of $\frac{1}{3}\ Z_\odot$ from near-IR spectroscopy, using the approximate R_{23} method (e.g., Kobulnicky, Kennicutt, & Pizagno 1999). This value agrees with other independent determinations: Leitherer (1999) used the relation between the equivalent widths of strong UV lines and the oxygen abundance to suggest LMC/SMC-like abundance in MS 1512-cB58. Pettini et al. (2000) analyzed weak interstellar absorption lines of Si II, S II, and Ni II to infer an abundance of about $\frac{1}{4}\ Z_\odot$. Heap et al. (1999) modeled the stellar wind lines in the spectrum of MS 1512-cB58 and found a metallicity like that in the SMC. Here we propose a new technique: *stellar photospheric lines* in the UV spectrum. This method was successfully used to estimate the metal abundance in hot stars by Haser et al. (1998) but has not been applied before to integrated spectra of star-forming galaxies. Photospheric lines in the UV may not allow abundance determinations as precise as those from optical nebular emission lines, but they can certainly be very useful when the optical wavelength range is inaccessible to observations.

The key spectral region between 1400 and 1440 Å is shown in Figure 11. The 1425 index defined in the previous section is in this wavelength region. The spectrum of MS 1512-cB58 is compared to two model spectra at $Z_\odot$ and $\frac{1}{4}\ Z_\odot$, both calculated for continuous star formation with age 100 Myr and Salpeter IMF from 1 to 100 $M_\odot$. This corresponds to the parameters derived by Pettini et al. (2000). However, the strength of the photospheric lines—as opposed to the wind lines—does not strongly depend on these specific parameters, as demonstrated in Figure 8. The 1425 index at $\frac{1}{4}\ Z_\odot$ and $Z_\odot$ metallicity has a value of 0.4 and 1.5 Å, respectively. It is obvious that the model with solar composition is a rather poor match to the observed spectrum. The low-metallicity model fits the observations rather well. The comparison in Figure 11 suggests that the newly formed stars in MS 1512-cB58 have a chemical composition similar to that of the LMC/SMC library stars.

A full comparison between the models and observations of MS 1512-cB58, including the stellar wind lines, is performed in Figure 12. The structure of this figure is identical to that for NGC 5253 (Fig. 10). The models shown are those of Figure 11. *Before comparing models and observations, one should recall that the narrow interstellar components, including those superposed upon the broad stellar wind lines, are not intended to be reproduced by the models.* The overall spectral fit with the low-Z library is much improved over that with solar composition. Apart from the better fit to the photospheric lines discussed before, there is a significant improvement in the modeling of the wind absorption components. At solar chemical composition, a blue absorption wing to Si IV λ1400 is predicted but not observed. This wing is not

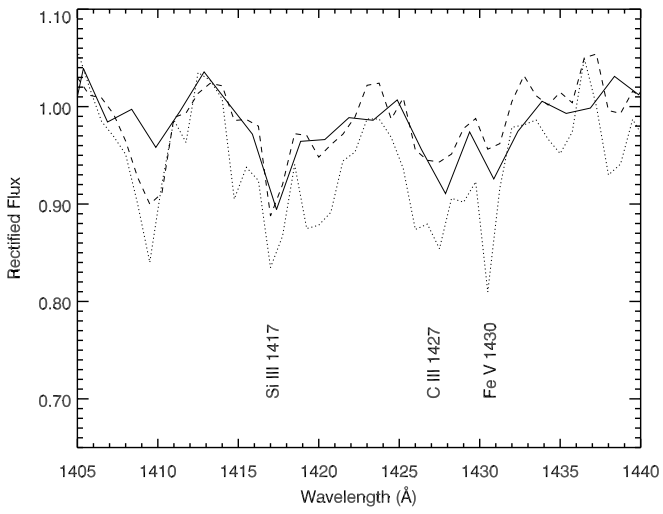

FIG. 11.—Spectral region around the photospheric features Si III λ1417, C III λ1427, and Fe V λ1430. *Solid line*: Observed spectrum of MS 1512-cB58; *dashed line*: model with $Z = \frac{1}{4}\ Z_\odot$; *dotted line*: model with $Z = Z_\odot$. Model parameters: continuous star formation with age 100 Myr and Salpeter IMF between 1 and 100 $M_\odot$.

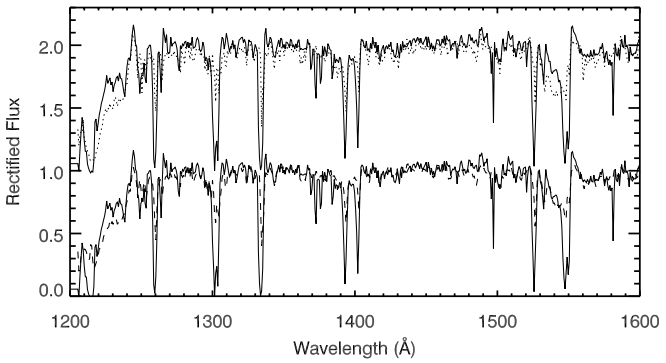

FIG. 12.—Comparison between the observed spectrum of MS 1512-cB58 (*solid lines*) and two synthetic models at $Z = \frac{1}{4}\ Z_\odot$ (*lower; dashed line*) and $Z = Z_\odot$ (*upper; dotted line*). The models have continuous star formation, age 100 Myr, and Salpeter IMF between 1 and 100 $M_\odot$.

present at $\frac{1}{4}\ Z_\odot$. Even more strikingly, the gross mismatch between the observed and theoretical C IV λ1550 absorption at $Z_\odot$ almost disappears at low metallicity—a clear indication of the lower than solar metallicity of MS 1512-cB58. The relative strength of the C IV λ1550 absorption to the emission of this and other wind lines is useful as a metallicity indicator: the absorption decreases with lower Z, all other galaxy properties being equal.

The properties of the stellar content of MS 1512-cB58 derived with the low-metallicity library are not significantly different from those derived before with the $Z_\odot$ library. Assuming constant star formation, the stellar wind profiles decrease in strength very slowly and essentially monotonically after about 5 Myr (see Fig. 9). In this case, only the IMF determines the relative proportion of O and B stars and, consequently, the line strength. A flatter IMF produces stronger emission and absorption. The C IV λ1550 profile is a very sensitive diagnostic: the model somewhat underpredicts the emission and overpredicts the wind absorption blueward of the deep interstellar line. Changing the IMF would always improve the fit to either component at the expense of the other. A Salpeter IMF is a reasonable tradeoff in order to achieve a reasonable overall fit.

We experimented with more complicated star formation histories in order to improve the fit. The C IV profile in MS 1512-cB58 has relatively strong emission relative to the absorption. The sequence in Figure 9 indicates that no continuous model at any age would fully match the observations. A flatter IMF would produce a *ratio* required by the observations, but emission and absorption would be much too strong. Inspection of Figure 6 suggests a possible scenario: an instantaneous starburst produces luminous O supergiants at 3–5 Myr after the burst. Such stars have the maximum emission/absorption ratio possible. If such a burst is combined with an older population in order to dilute both the emission and absorption, an excellent fit to the observations can be constructed. We verified that this is indeed the case: a 4 Myr–old burst with a flat IMF, superposed upon a 1 Gyr–old population with constant star formation and a steep IMF, provides a much better fit than the model shown in Figure 12. However, this is a somewhat academic exercise and would not add new insight already gained from the standard model: MS 1512-cB58 has a metallicity of $\frac{1}{4}\ Z_\odot$ and is currently experiencing a powerful starburst producing massive stars down to at least 10 $M_\odot$ and following a more or less standard IMF.

Could the mismatch between the observed and theoretical C IV λ1550 profiles be caused by an abundance effect? Decreasing the carbon abundance will affect mostly the absorption and leave the emission relatively unchanged. This is the trend we found from Galactic to LMC/SMC abundances, and we suspect—but have no observational proof—that the trend continues. Our test using zero-metallicity B stars provides tentative support for this hypothesis (see Fig. 5). The C IV absorption is indeed weaker in the test spectrum of Figure 5. On the other hand, zero-metallicity B stars generate no excited Si II λ1265, a line that is clearly present in MS 1512-cB58 and that is nicely reproduced by our model in Figure 12. The carbon abundance of the library stars is the result of the chemical history of the Magellanic Clouds. A priori, there is no reason why the chemical evolution of MS 1512-cB58 should be identical to that of the Magellanic Clouds. Since MS 1512-cB58 is likely to be at a relatively early stage of evolution, given its redshift, fewer generations of low- and intermediate-mass stars could have formed. Since these stars are responsible for the carbon production, chemical evolution models predict an underabundance of carbon relative to elements predominantly formed in massive stars, like oxygen (Bradamante, Matteucci, & D'Ercole 1998). However, the C III λ1427 line in MS 1512-cB58 shows no peculiarity (see Fig. 11). Its strength, both in absolute terms and relative to Si III λ1417 and Fe V λ1430, is approximately the same as in the model spectrum. This suggests that intermediate-mass stars may have had sufficient time to evolve and release carbon in MS 1512-cB58.

6. CONCLUSIONS

The new low-metallicity library complements our previous model spectra based on solar metallicity stars and allows an important extension of the parameter space available for study. Galaxies with metallicity close to that of the SMC and with correspondingly low mass and luminosity can be modeled. We find that metallicity affects the UV spectrum, but not in a dramatic way. Therefore, previous studies, which compared observed spectra of metal-poor galaxies to models with solar metallicity library stars, are still approximately valid.

What improvements could be made in the future? Pushing the library toward significantly lower metallicities is out of reach. The only other very metal-poor galaxy in the Local Group with a significant massive-star population is IC 1613 (Armandroff & Massey 1985). The metallicity of this irregular galaxy is half that of the SMC (Cole et al. 1999). At a distance of 400 kpc, the brightest O stars are 3 mag fainter than their cousins in the SMC. The corresponding increase of the observational effort to define an optical sample and subsequently accumulate a body of UV spectra can hardly be justified in view of the incremental increase of the parameter space.

Two significant enhancements of the library can be accomplished at a modest observational expense. First, extension of the spectral type coverage to late B stars would allow us to apply the spectral synthesis analysis to galaxies at evolutionary stages when stars with masses as low as 5 $M_\odot$ become important. Spectral features of such stars are already contributing to the spectrum of, e.g., MS 1512-cB58, and they become dominant in more evolved systems such as poststarburst galaxies. A second enhancement would be the extension of the wavelength coverage to longer wave-

lengths, both at low and high metallicity. B stars in particular have important diagnostics between 1600 and 3000 Å, such as Al III λ1860 and Si III λ1892 (Walborn, Parker, & Nichols 1995b).

The synthetic UV spectra at low metallicity are part of Starburst99 (Leitherer et al. 1999). This application allows users to generate tailored models using a Web-based interface.[3] The original Starburst99 package has been updated to incorporate the models described in this paper. Users can generate their models via the "Run a simulation" page by specifying the low-metallicity library. In addition, a set of model spectra with standard stellar population parameters is available for download from the same Web site.

[3] Available at the URL http://www.stsci.edu/science/starburst99.

João Leão acknowledges support from the Space Telescope Science Institute Summer Student Program. We are grateful to Nolan Walborn for providing comments on an earlier version of the manuscript. This work was supported by *HST* grant GO-07437.01-96A from the Space Telescope Science Institute, which is operated by the Association of Universities for Research in Astronomy, Inc., under NASA contract NAS5-26555.

REFERENCES

Armandroff, T. E., & Massey, P. 1985, ApJ, 291, 685
Azzopardi, M., & Vigneau, J. 1975, A&AS, 22, 285
———. 1982, A&AS, 50, 291
Bradamante, F., Matteucci, F., & D'Ercole, A. 1998, A&A, 337, 338
Brunet, J. P., Imbert, N., Martin, N., Mianes, P., Prevot, L., Rebeirot, E., & Rousseau, J. 1975, A&AS, 21, 109
Calzetti, D., Meurer, G. R., Bohlin, R. C., Garnett, D. R., Kinney, A. L., Leitherer, C., & Storchi-Bergmann, T. 1997, AJ, 114, 1834
Cole, A. A., et al. 1999, AJ, 118, 1657
Conti, P. S., Garmany, C. D., & Massey, P. 1986, AJ, 92, 48
Conti, P. S., Leitherer, C., & Vacca, W. D. 1996, ApJ, 461, L87
Crampton, D. 1979, ApJ, 230, 717
de Mello, D., Leitherer, C., & Heckman, T. M. 2000, ApJ, 530, 251
Dey, A., van Breugel, W., Vacca, W. D., & Antonucci, R. 1997, ApJ, 490, 698
Drew, J. 1990, in ASP Conf. Ser. 7, Properties of Hot Luminous Stars, ed. C. D. Garmany (San Francisco: ASP), 230
Ebbels, T. M. D., Le Borgne, J.-F., Pelló, R., Ellis, R. S., Kneib, J.-P., Smail, I., & Sanahuja, B. 1996, MNRAS, 281, L75
Ellingson, E., Yee, H. K. C., Bechtold, J., & Elston, R. 1996, ApJ, 466, L71
Garmany, C. D., & Conti, P. S. 1984, ApJ, 284, 705
Garmany, C. D., Conti, P. S., & Massey, P. 1987, AJ, 93, 1070
Garnett, D. R. 1999, in IAU Symp. 190, New Views of the Magellanic Clouds, ed. Y.-H. Chu, N. Suntzeff, J. Hesser, & D. Bohlender (San Francisco: ASP), 266
Haser, S. M., Pauldrach, A. W. A., Lennon, D. J., Kudritzki, R.-P., Lennon, M., Puls, J., & Voels, S. A. 1998, A&A, 330, 285
Heap, S. R., Bouret, J.-C., Hubeny, I., & Lanz, T. M. 1999, BAAS, 195, 919
Heckman, T. M., & Leitherer, C. 1997, AJ, 114, 69
Heckman, T. M., Robert, C., Leitherer, C., Garnett, D. R., & van de Rydt, F. 1998, ApJ, 503, 646
Howk, J. C., & Sembach, K. R. 2000, AJ, 119, 2481
Johnson, K. E., Vacca, W. D., Leitherer, C., Conti, P. S., & Lipscy, S. J. 1999, AJ, 117, 1708
Kinney, A. L., Bohlin, R. C., Calzetti, D., Panagia, N., & Wyse, R. F. G. 1993, ApJS, 86, 5
Kinney, A., Calzetti, D., Bohlin, R. C., McQuade, K., Storchi-Bergmann, T., & Schmitt, H. R. 1996, ApJ, 467, 38
Kobulnicky, H. A., Kennicutt, R. C., & Pizagno, J. L. 1999, ApJ, 514, 544
Kudritzki, R.-P. 1998, in Stellar Astrophysics for the Local Group, ed. A. Aparicio, A. Herrero, & F. Sánchez (Cambridge: Cambridge Univ. Press), 149
Lamers, H. J. G. L. M., Haser, S., de Koter, A., & Leitherer, C. 1999, ApJ, 516, 872
Lamers, H. J. G. L. M., Snow, T. P., & Lindholm, D. M. 1995, ApJ, 455, 269
Leitherer, C. 1999, in Chemical Evolution From Zero To High Redshift, ed. J. R. Walsh & M. R. Rosa (New York: Springer), 204
———. 2001, in A Decade of *HST* Observations, ed. M. Livio, K. S. Noll, & M. Stiavelli (Cambridge: Cambridge Univ. Press), in press
Leitherer, C., Robert, C., & Heckman, T. M. 1995, ApJS, 99, 173
Leitherer, C., et al. 1999, ApJS, 123, 3
Lowenthal, J. D., et al. 1997, ApJ, 481, 673
Mas-Hesse, J. M., & Kunth, D. 1999, A&A, 349, 765
Massey, P., Parker, J. W., & Garmany, C. D. 1989, AJ, 98, 1305
Nemry, F., Surdej, J., & Herniaz, A. 1991, A&A, 247, 469
Pauldrach, A. W. A., Kudritzki, R.-P., Puls, J., & Butler, K. 1990, A&A, 228, 125
Pettini, M., Steidel, C. C., Adelberger, K. L., Dickinson, M., & Giavalisco, M. 2000, ApJ, 528, 96
Plante, S. 1998, in ASP Conf. Ser. 147, Abundance Profiles: Diagnostic Tools for Galaxy History, ed. D. Friedli, M. Edmunds, C. Robert, & L. Drissen (San Francisco: ASP), 192
Robert, C. 1996, in ASP Conf. Ser. 98, From Stars To Galaxies: The Impact of Stellar Physics on Galaxy Evolution, ed. C. Leitherer, U. Fritze-v. Alvensleben, & J. P. Huchra (San Francisco: ASP), 133
———. 1999a, in IAU Symp. 193, Wolf-Rayet Phenomena in Massive Stars and Starburst Galaxies, ed. K. A. van der Hucht, G. Koenigsberger, & P. R. J. Eenens (San Francisco: ASP), 616
———. 1999b, in ASP Conf. Ser. 192, Spectrophotometric Dating of Stars and Galaxies, ed. I Hubeny, S. R. Heap, & R. H. Cornett (San Francisco: ASP), 16
Robert, C., Leitherer, C., & Heckman, T. M. 1993, ApJ, 418, 749
Sanduleak, N. 1969, Contrib. Cerro Tololo Inter-American Obs. 89
Schaller, G., Schaerer, D., Meynet, G., & Maeder, A. 1992, A&AS, 96, 269
Schmidt-Kaler, T. 1982, in Landolt-Börnstein, New Series, Group VI, Vol. 2b, ed. K. Schaifers & H. H. Voigt (Berlin: Springer), 1
Seitz, S., Saglia, R. P., Bender, R., Hopp, U., Belloni, P., & Ziegler, B. 1998, MNRAS, 298, 945
Sekiguchi, K., & Anderson, K. S. 1987a, AJ, 94, 129
———. 1987b, AJ, 94, 644
Smartt, S. J., & Rolleston, W. R. J. 1997, ApJ, 481, L47
Steidel, C. C., Giavalisco, M., Pettini, M., Dickinson, M., & Adelberger, K. L. 1996, ApJ, 462, L17
Teplitz, H. I., et al. 2000, ApJ, 533, L65
Tremonti, C. A., Calzetti, D., Leitherer, C., & Heckman, T. M. 2001, ApJ, submitted
Vacca, W. D., Garmany, C. D., & Shull, J. M. 1996, ApJ, 460, 914
Walborn, N. R., Lennon, D. J., Haser, S. M., Kudritzki, R.-P., & Voels, S. A. 1995a, PASP, 107, 104
Walborn, N. R., Lennon, D. J., Heap, S. R., Lindler, D. J., Smith, L. J., Evans, C. J., & Parker, J. W. 2000, PASP, 112, 1243
Walborn, N. R., Nichols-Bohlin, J., & Panek, R. J. 1985, International Ultraviolet Explorer Atlas of O-type Spectra from 1200 to 1900 Å (Washington: NASA)
Walborn, N. R., & Panek, R. J. 1984, ApJ, 280, L27
Walborn, N. R., Parker, J. W., & Nichols, J. S. 1995b, International Ultraviolet Explorer Atlas of B-type Spectra from 1200 to 1900 Å (Washington, DC: NASA)
Yee, H. K. C., Ellingson, E., Bechtold, J., Carlberg, R. G., & Cuillandre, J.-C. 1996, AJ, 111, 1783